MANUSCRIPT FOR PUBLICATION

Comparing Artificial Intelligence Cephalometric Tracings in Orthodontic Software Packages

Authors: Dominica Portman D.M.D.[1]
Mark Hans D.D.S., M.S.D.[2]
Juan Martin Palomo D.D.S., M.S.D.[3]
Orhan Ozguner, B.S., M.S., Ph.D[4]
Tarek Elshebiny D.D.S., M.S.D.[5]

1. Resident, Department of Orthodontics, Case Western Reserve University, Cleveland, OH, USA
2. Chair, Department of Orthodontics, Case Western Reserve University, Cleveland, OH, USA
3. Professor and Program Director, Department of Orthodontics, Case Western Reserve University, Cleveland, OH, USA
4. Assistant Professor, Department of Computer and Data Sciences, Case Western Reserve University, Cleveland, OH, USA
5. Assistant Professor and Clinical Director, Department of Orthodontics, Case Western Reserve University, Cleveland, OH, USA

Corresponding Author:

Tarek ElShebiny
Case Western Reserve University
School of Dental Medicine
Department of Orthodontics
9601 Chester Avenue
Cleveland, OH 44106
Tme18@case.edu

Comparing Artificial Intelligence Cephalometric Tracings in Orthodontic Software Packages

ABSTRACT

OBJECTIVE: The purpose of this study is to compare four different software programs, CephX, iOrtho, OrthoDx, and Webceph, in the automatic landmark detection of 2D cephalometric radiographs by evaluating the envelope of errors of each landmark.

MATERIALS AND METHODS: Thirty 2D cephalometric radiographs from the American Association of Orthodontists Foundation (AAOF) were downloaded as full-resolution images from the AAOF.org website. All thirty radiographs were pre-orthodontic treatment and collected from the Matthews collection. Each radiograph was uploaded to the following orthodontic imaging software programs: CephX, iOrtho, OrthoDx, and Webceph for automatic AI-based landmark identification of the following anatomic points: Sella (S), Nasion (Na), Orbitale (Or), A point (A), U1A (U1 apex), U1E (U1 incisal edge), L1E (L1 incisal Edge), L1A (L1 apex), B point (B), Pogonion (P), Menton (Me), and Porion (Po). Once complete, each radiograph was uploaded onto Dolphin Imaging, and each AI-populated landmark was digitally traced to obtain the X,Y coordinates. To find the envelopes of error for each landmark, scattergrams were plotted after the means were subtracted from the raw X,Y coordinates. Then, standard deviations of each landmark were calculated.

RESULTS: All of the AI-traced landmarks in this study were plotted in scatterplots to show variability from the mean. Each AI-traced scattergram demonstrated greater variability than

human tracers. In addition, in regards to the standard deviations, when compared to human tracers, AI was not as accurate in finding the X,Y coordinates of each landmark.

Conclusion: AI-based landmark identification of 2D cephalometric radiographs show great variability compared to human tracers. Thus, clinicians should not rely solely on AI-based modalities to evaluate radiographs.

Introduction:

Cephalometric imaging has been the foundation of research and treatment planning in orthodontics since its introduction in 1931[1]. It has allowed clinicians to plan treatments based on the facial skeleton rather than relying merely on the patient's soft tissue and teeth[2,3]. In 1953, Cecil Steiner stated that, "it is my opinion that roentgenographic cephalometry is one of the most important contributions to the progress in orthodontics"[4].

The importance of cephalometric analysis as a diagnostic tool in orthodontics is still apparent almost 100 years after its introduction[2]. Cephalometrics aid clinicians in analyzing the relationship between the maxilla, the mandible, the cranial base, and the teeth [5]. Once the data is gathered, deviations from an average in skeletal and dentoalveolar morphology are assessed, and this determines whether a malocclusion can be attributed to a skeletal or dentoalveolar deviation. Moreover, dental compensations or dysplastic growth in patients with a skeletal discrepancy can also be determined. Thus, even in modern orthodontics, analyzing lateral cephalograms is very valuable during the treatment planning phase.

Traditional methods of analysis required the clinician to manually trace skeletal and dental landmarks and determine linear and angular measurements by using rulers and protractors[2]. This method was likely to produce errors in radiograph magnification, landmark identification, tracing and measuring [6--9]. A study conducted by Baumrind and Frantz (1971) aimed to find the range of operator variation in traced cephalograms in the orthodontic practice [6]. A sample of 20 lateral head films were randomly selected

and traced by 5 clinicians. The study concluded that the magnitude of error varies greatly from landmark to landmark, and that the distribution of error for most landmarks usually follow a noncircular pattern. For example, points such as Orbitale and A-point had a more linear pattern of error, indicating more variation between operators. Therefore, they are classified as more difficult landmarks to locate. On the other hand, points such as Sella and Porion had a small envelope of error, resembling more of a circle, indicating less variation between operators.

While the findings of the Baumrind study still hold true today, the main difference in cephalometric analysis is in how angular and linear measurements are detected after landmark identification. Cephalometric imaging softwares automatically determine angular and linear measurements after the clinician manually locates the appropriate landmarks. Previous studies have found that this computer-aided cephalometric analysis does not introduce more error than traditional hand-tracing methods [10-13]. However, intra- and inter-observer errors may persist in digital landmark identification [14-15].

Although an estimated 97.3% of orthodontists in the United States routinely take pre-treatment lateral cephalometric radiographs [16], it has been documented that an experienced clinician can take up to 15 minutes to manually identify landmarks in imaging software programs [17-18]. Due to the time-consuming nature of manual landmark identification, many clinicians do not trace lateral cephalometric radiographs, but rather, take them as it is considered the standard of care [19-21]. This lack of radiographic pre-treatment analysis and the lack of superimposition comparison at the conclusion of orthodontic treatment may lead to inaccurate diagnosis and treatment planning. As a result, orthodontic software companies are

now looking to implement artificial intelligence (AI) modalities in lateral cephalometric analysis. Further research is needed to assess the accuracy and reliability of these modalities without human intervention.

Methods:

This retrospective study examined the 2-dimensional cephalometric records of 30 patients from the American Association of Orthodontics Foundation (AAOF) Matthew's collection. The institutional review board at Case Western Reserve University (CWRU) approved this study. Subjects were selected based on adequate pretreatment cephalograms. No informed consent was needed for this study.

The inclusion criteria for this study were as follows: (1) subjects had at least first mandibular and maxillary first molars fully erupted, (2) subjects had upper and lower incisors fully erupted, (3) subject radiographs were taken before orthodontic treatment, (4) subjects who did not have craniofacial deformities. The exclusion criteria for this study were as follows: (1) subjects that were in orthodontic treatment, (2) subjects without the first maxillary and mandibular molars fully erupted, (3) subjects without the upper and lower incisors fully erupted, (4) subjects with craniofacial deformities.

Each of the 30 radiographs were downloaded from the AAOF.org website to obtain a full-resolution image. Each radiograph was uploaded to the following orthodontic imaging software programs for automatic AI-based landmark identification: CephX, iOrtho, OrthoDx, and Webceph. After the AI-based automatic tracing was complete, the images were uploaded to Dolphin Imaging software where one investigator (DP) digitally traced each AI-populated point to obtain the X,Y coordinates of each landmark. The following anatomic landmarks were used: Sella (S), Nasion (Na), Orbitale (Or), A point (A), U1A (U1 apex), U1E (U1 incisal edge),

L1E (L1 incisal Edge), L1A (L1 apex), B point (B), Pogonion (P), Menton (Me), and Porion (Po).

Scattergrams were generated for all twelve landmarks. Each scattergram included 120 points that were derived from subtracting the mean of the four sets of X and Y coordinates from the AI-traced X and Y coordinates for each landmark. In other words, the 120-point scattergrams were derived from the thirty lateral cephalometric radiographs, traced by four AI programs, and included twelve landmarks. Each scattergram represented the dispersion of estimating errors for a single landmark around the mean of each landmark. The scale of each scattergram was 1.0 mm and were correctly proportioned as to size.

Error Study

Digitization error for each group was accounted for by randomly selecting ten radiographs to be traced for a second time after the AI-based tracings were completed. All twelve landmarks were assessed a second time via their X,Y coordinates. The two sets of tracings were then compared using intraclass correlation coefficients. All measurements showed great reproducibility with high intra-class reliability (>0.97).

Results:

Figures 1-12 are enlarged representations of the twelve scattergrams. From the scattergrams, we can see that there are large differences in variability of estimation among the landmarks, and that porion and lower 1 apex have the greatest variability. Additionally, examination of the scattergrams shows that the distributions of error for most landmarks vary in the X and Y directions. For example, Figure 1 demonstrates that the estimates of porion

are dispersed primarily along the horizontal, or X, axis, while the estimates for sella in Figure 2 are dispersed primarily along the vertical, or Y, axis. For this reason, the X and Y values of the total variance for each of the twelve landmarks were found, resulting in distinct standard deviations in the X and Y planes (tables 9 and 10).

Simple statistics for the data means, standard deviations and standard errors are included in tables 9 and 10. Table 9 shows the measures of dispersion for skeletal landmarks, while table 10 shows the measures of dispersion for the dental landmarks. The landmarks are arranged in order of increasing magnitude of error. Column 1 of tables 9 and 10 lists the standard deviations for the total error distributions for each landmark. However, as previously noted, it is important to note that the variability depends on each landmark, as some landmarks vary more in the horizontal (X) or vertical (Y) direction.

All standard deviations in this study were calculated using the following formula:

$$S = \sqrt{\frac{\sum d^2}{N(K-1)}}$$

Where d = the deviation of one tracing value from the mean value for that landmark for that film, N = the number of lateral cephalometric radiographs (in the current study, *30*), K = the number of tracings per headfilm (in the current study, *4*).

Discussion:

Alleviating the clinician's workload in performing labor-intensive tasks has become a significant focus in modern orthodontics. Among the recent advancements, AI-driven automatic landmark detection and subsequent tracing represent a notable development. This study aimed to evaluate the error margins associated with

automatic AI-based landmark detection on 2D cephalometric radiographs across four distinct orthodontic imaging software platforms.

This study was inspired by the work of Baumrind in 1971, which employed scatterplots to evaluate the envelope of error in 2D cephalograms. However, in Baumrind's investigation, five independent examiners traced 20 lateral cephalograms, while in this study, we used four orthodontic imaging software programs and 30 lateral cephalograms.

We will now breakdown the similarities and differences between Baumrind's findings and this study.

Porion, Figure 2. In the Baumrind study, porion was defined as the machine porion, whereas the AI-based tracings utilized the anatomical porion. Anatomical porion is widely recognized as a challenging landmark to identify due to the limited contrast present in radiographs. While Baumrind's machine porion yielded consistent and circular identification by human tracers, the AI-based tracings demonstrated considerable variability in both X and Y coordinates, with particularly pronounced differences in the horizontal (X) direction. Furthermore, in the present study, porion exhibited the highest variability with regard to the envelopes of error.

Sella, Figure 3. Sella involves visual estimations of the center of a structure, so performance here was very good for the human tracers in the Baumrind study. In our study, Sella had an obvious concentration of points in the center, but had large variations in the vertical, or Y, direction than humans.

Orbitale, Figure 4. Baumrind defined the orbitale landmark as the "most prominent" orbit, a designation that may have been influenced by variability in human

tracers' subjective interpretations. This subjectivity likely contributed to the greater dispersion observed in their scattergram. Although AI lacks subjective bias, it may also have encountered challenges in consistently identifying the "most prominent" orbit. This is evidenced by the lack of a clear concentration around the center, as was more observed with the sella landmark. Therefore, challenges for AI in the horizontal and vertical directions were apparent.

Nasion, Figure 5. Nasion holds significant importance as many orthodontic analyses rely on angular measurements based on the S-N plane. In the Baumrind study, while the estimates for nasion were generally accurate, a substantial number of gross errors were observed. These errors likely stemmed from human tracers misidentifying entirely different anatomical structures. In the current study, similar to orbitale, there was no distinct clustering around the mean for nasion, indicating variability in its identification in both the horizontal (X) and vertical (Y) directions.

A point, Figure 6; B point, Figure 7. The identification of A and B points demonstrated greater variability among human tracers compared to the previously discussed landmarks. This variability was moreso in the vertical (Y) direction. However, AI-based tracings exhibited less variability for A and B points compared to nasion and orbitale. Additioannly, AI had the opposite difficulty in identifying these points: greater envelopes of error in the horizontal plane, indicating more difficulty in identifying these points in the antero-posterior direction. According to Baumrind, the increased variability among human tracers when estimating landmarks on curved structures, such as A or B point, arises from the tendency of errors to be larger and distributed along the bony edge or, more specifically, the surface of the skull. This inherent challenge in

accurately pinpointing the landmark contributes to the observed variability in A and B points.

Menton, Figure 8. Human tracers exhibited greater variability in identifying menton than anticipated, especially in the horizontal plane. Notably, a consistent trend was observed: while the AI-based tracings also demonstrated variability, the degree of variability for menton was lower compared to other landmarks such as orbitale and nasion, with more difficultly in the anteroposterior (X) plane, just like that found in A and B points, and to human tracers.

Pogonion, Figure 9. we see the trend continue with landmarks along the edge of the skull: more variabialilty, and difficulty in tracings in the opposite directions. Humans had more difficulty in the vertical plane, while AI had more difficulty in the horizontal plane.

Upper incisor apex, Figure 10; Lower incisor apex, Figure 12. Certain landmarks present challenges due to the significant "noise" introduced by adjacent structures, often leaving the observer to estimate the position of a point without direct physical evidence visible on the radiograph. The lower incisor apex exemplifies such a landmark. For the lower incisor apex, observers are frequently required to infer the location conceptually, relying on their general understanding of typical tooth length and taper, based on the shape of the crown and the visible portion of the root.

In making these conceptual estimations, the observer's prior experience plays a critical role; an experienced operator is likely to achieve greater reliability than a novice. While conceptual judgments are not inherently invalid, it is reasonable to expect them to exhibit greater variability compared to judgments made for clearly

discernible landmarks. Similarly, AI had great variability in both the X and Y coordinates for lower incisor apex, as well as the X coordinates for upper incisor apex.

Upper incisor edge, Figure 11; Lower incisor edge, Figure 13. The Baumrind study demonstrated high accuracy in estimating landmarks where the edges of the image exhibit sharp, well-defined contours, such as the upper and lower incisor edges. Similarly, the AI-based tracings showed reduced variability in identifying incisor edges compared to the apex. However, considerable variability was still observed, particularly in the horizontal (X-axis) direction.

Conclusion:

In this retrospective study, the hypothesis that AI-based modalities in orthodontic imaging software exhibit no variability across landmarks was rejected for all evaluated landmarks. The degree of variability, however, was not uniform. AI often encountered challenges in identifying either the vertical or anteroposterior (AP) coordinates of specific landmarks. For instance, difficulties with horizontal (X-axis) localization were observed for landmarks such as porion, A and B points, menton, pogonion, and the upper and lower incisal edges. Conversely, vertical (Y-axis) localization posed challenges for landmarks such as sella, whereas orbitale and nasion displayed relatively comparable envelopes of error in both horizontal and vertical dimensions.

Although AI-based tracing modalities enhance efficiency and save time in orthodontic practices, clinicians should exercise caution and avoid relying exclusively on this technology without human oversight.

TABLE 1: Measures of Dispersion: Skeletal Landmarks

A. Skeletal Landmarks			
	SD[a]	**SDx[b]**	**SDy[c]**
1. SELLA	3.2	1.82	2.63
2. POINT A	3.51	3.1	1.65
3. POINT B	4.12	3.67	1.87
4. MENTON	4.78	4.42	1.82
5. NASION	4.98	4.1	2.84
6. ORBITALE	5.09	4.4	2.56
7. POGONION	7.18	6.89	2.01
8. PORION	14.22	12.6	6.6

a *STANDARD DEVIATION FOR TOTAL ERROR*

b *STANDARD DEVIATION FOR ERROR IN HORIZONTAL DIRECTION*

c *STANDARD DEVIATION FOR ERROR IN VERTICAL DIRECTION*

TABLE 2: Measures of Dispersion: Dental Landmarks

B. Dental Landmarks			
	SD[a]	**SD_X[b]**	**SD_y[c]**
1. UPPER 1 INCISAL EDGE	3.54	3.2	1.52
2. LOWER 1 INCISAL EDGE	3.9	3.46	1.8
3. UPPER 1 APEX	3.92	3.2	2.26
4. LOWER 1 APEX	4.83	4.12	2.52

a *STANDARD DEVIATION FOR TOTAL ERROR*

b *STANDARD DEVIATION FOR ERROR IN HORIZONTAL DIRECTION*

c *STANDARD DEVIATION FOR ERROR IN VERTICAL DIRECTION*

FIGURE 1: SCHEMATIC OF A NETWORK

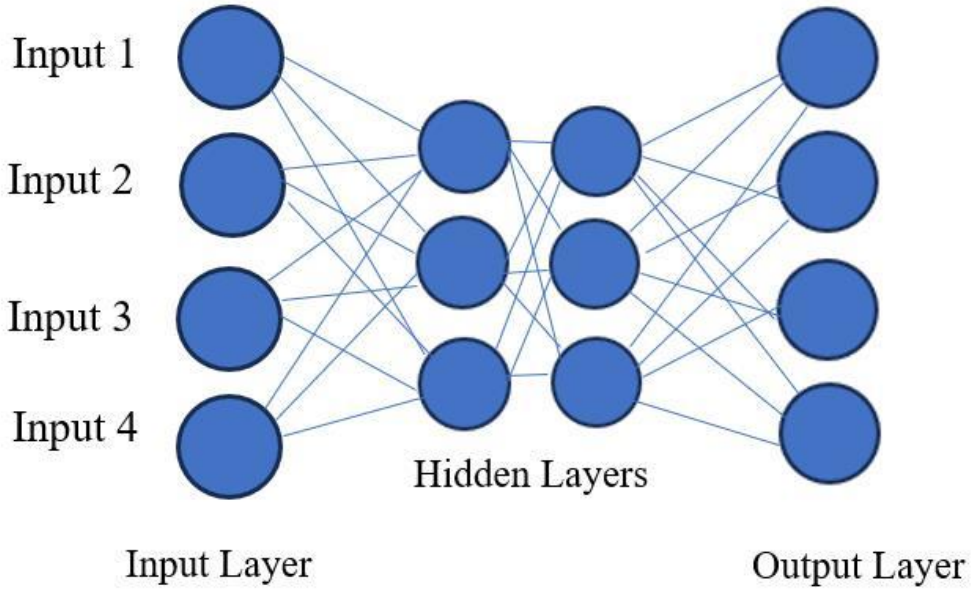


FIGURE 2: DISTRIBUTION OF ESTIMATING ERRORS; PORION

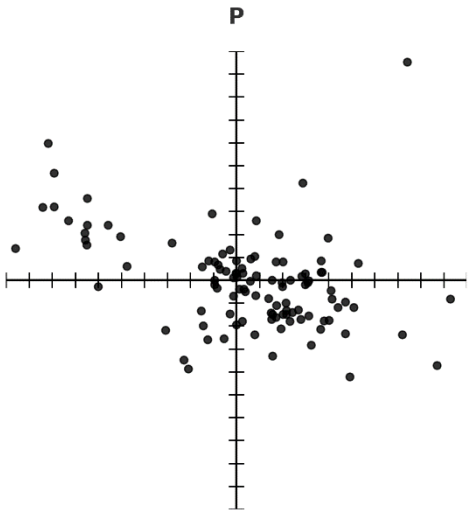


FIGURE 3: DISTRIBUTION OF ESTIMATING ERRORS; SELLA

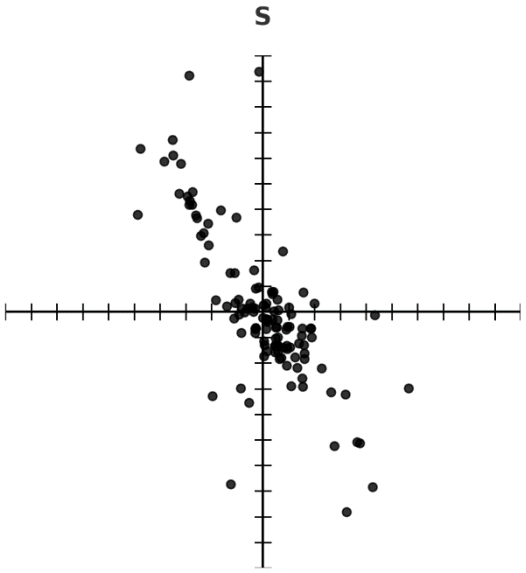


FIGURE 4: DISTRIBUTION OF ESTIMATING ERRORS; ORBITALE

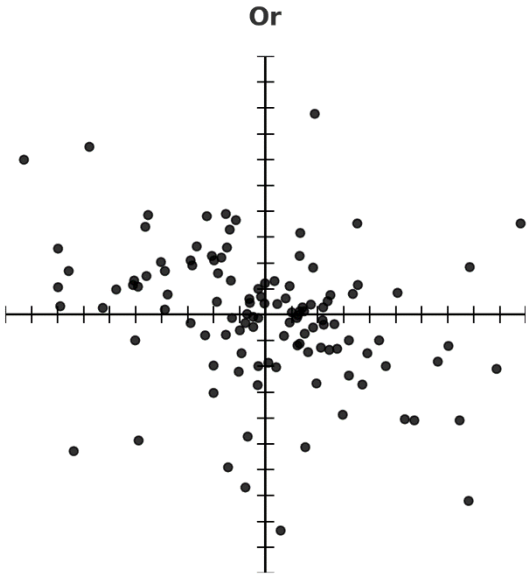


FIGURE 5: DISTRIBUTION OF ESTIMATING ERRORS; NASION

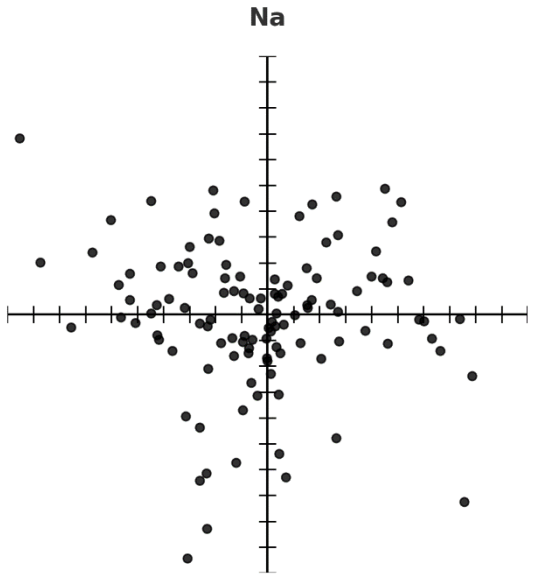


FIGURE 6: DISTRIBUTION OF ESTIMATING ERRORS; A POINT

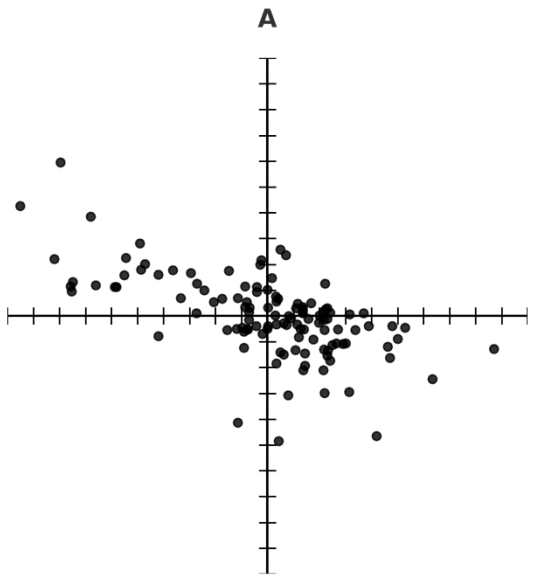


FIGURE 7: DISTRIBUTION OF ESTIMATING ERRORS; B POINT

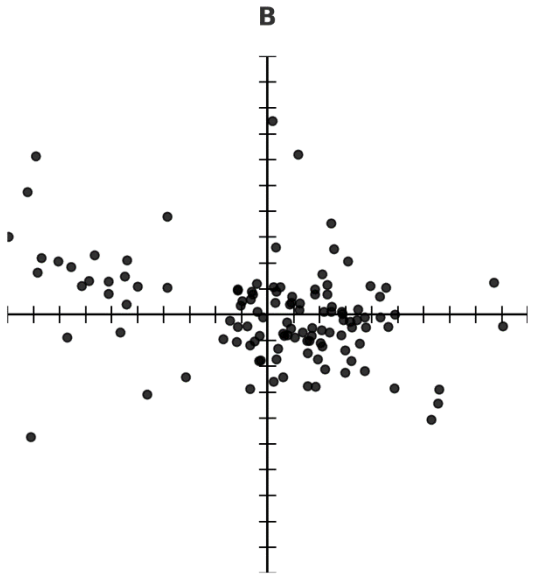


FIGURE 8: DISTRIBUTION OF ESTIMATING ERRORS; MENTON

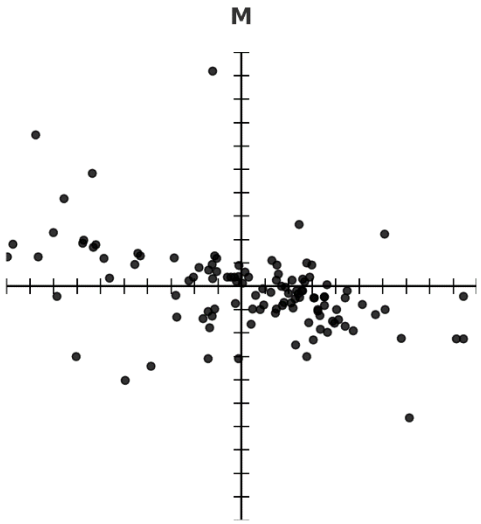


FIGURE 9: DISTRIBUTION OF ESTIMATING ERRORS; POGONION

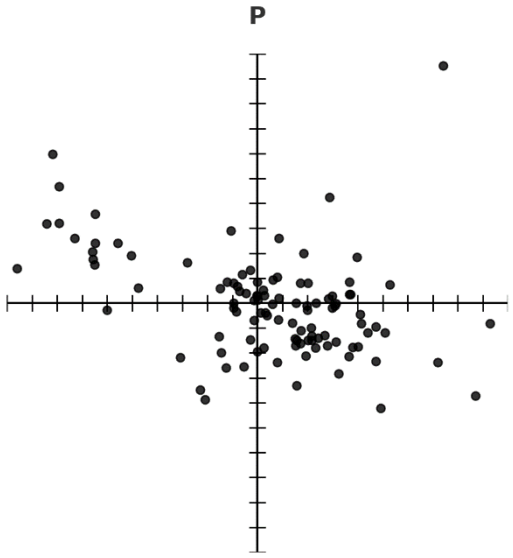


FIGURE 10: DISTRIBUTION OF ESTIMATING ERRORS; UPPER 1 APEX

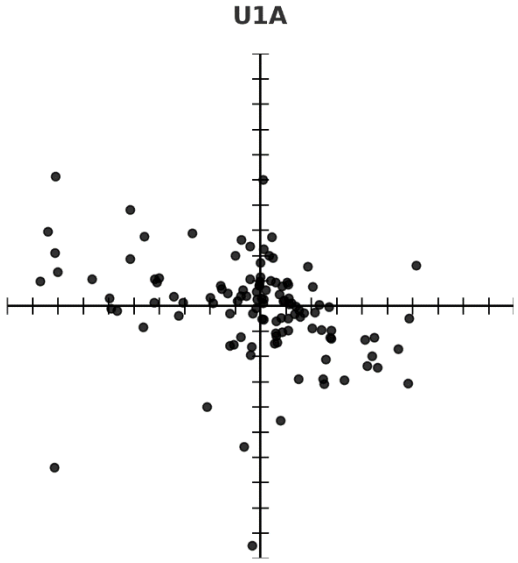


FIGURE 11: DISTRIBUTION OF ESTIMATING ERRORS; UPPER 1 INCISAL EDGE

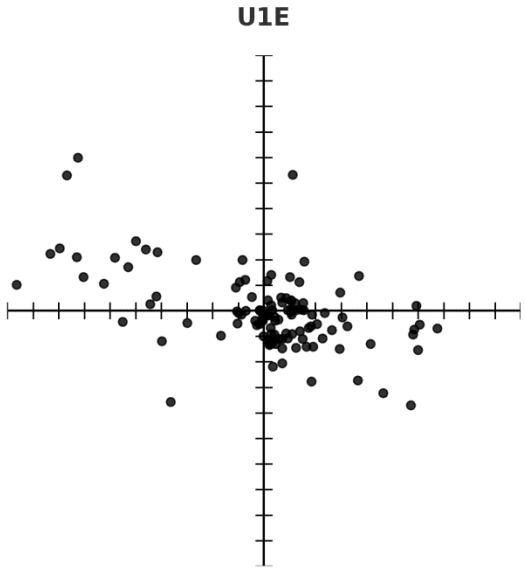


FIGURE 12: DISTRIBUTION OF ESTIMATING ERRORS; LOWER 1 APEX

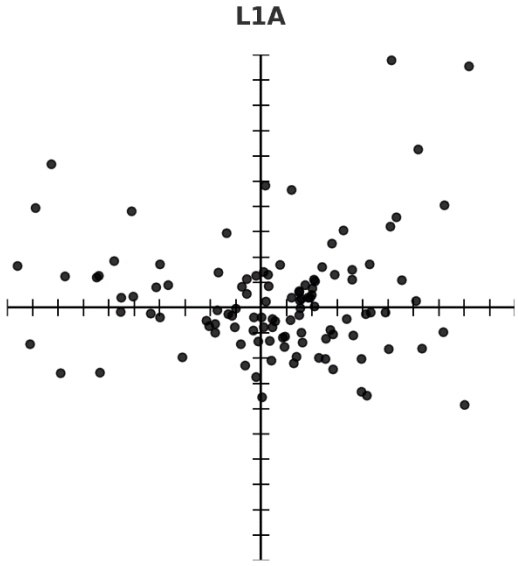
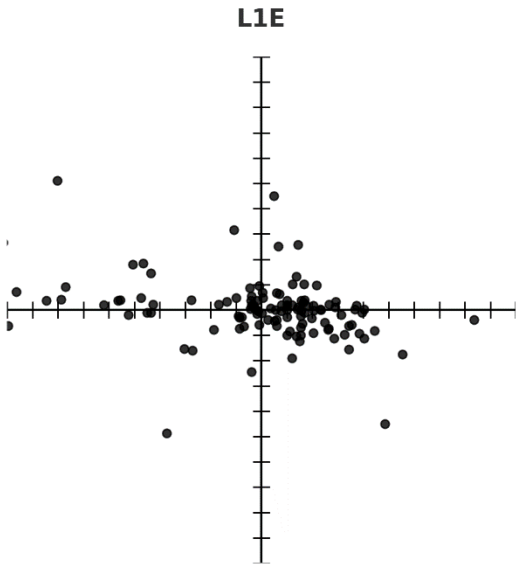


FIGURE 13: DISTRIBUTION OF ESTIMATING ERRORS; LOWER 1 INCISAL EDGE



Cited Literature

1. Broadbent BH. A new X- ray Technique and its application to orthodontia: The Introduction of Cephalometric Radiography.” Angle Orthodontist. 1931;1(2): 45-66.

2. Proffit WR, Fields HW, Larson B, Sarver DM. Contemporary Orthodontics-e-Book. Elsevier Health Sciences: Amsterdam, The Netherlands. 2018.

3. Broadbent BH. Bolton standards and technic in orthodontic procedures. Angle Orthodontist. 1937;(4):209e33.

4. Steiner CC. The use of cephalometrics as an aid to planning and assessing orthodontic treatment: report of a case. American Journal of Orthodontics. 1960;46(10): 721-735.

5. Graber L. Orthodontics Current Principles and Techniques. Philadelphia, PA: Mosby Elsevier; 2012.

6. Baumrind S, Frantz RC. The reliability of head film measurements 1. Landmark identification. American Journal of Orthodontics. 1971;60(2): 111-127.

7. Cohen AM, Linney AD. A low cost system for computer-based cephalometric analysis. British Journal of Orthodontics. 1986;13(2): 105–118.

8. Houston WJB. The analysis of errors in orthodontic measurements. American Journal of Orthodontics. 1983;83(5): 382–390.

9. Houston WJB, Maher RE, McElroy D, Sherriff M. Sources of error in measurements from cephalometric radiographs. European Journal of Orthodontics. 1986;8(3): 149–151.

10. Gravely JF, Benzies PM. The clinical significance of tracing error in cephalometry. British Journal of Orthodontics. 1974; 1(3): 95–101.

11. Jackson PH, Dickson G C, Birnie D J 1985 Digital image processing of cephalometric radiographs: a preliminary report. British Journal of Orthodontics 12: 122–132

12. Enlow DH, Hans MG. Essentials of facial growth. WB Saunders Company, Philadelphia, 1996; pp. 259–260.

13. Erkan M, Gurcan-Gurel H, Nur M, Demirel B. Reliability of four different computerized cephalometric analysis programs. European Journal of Orthodontics. 2012;34: 318-321.

14. Chen YJ, Chen SK, Chang HF, Chen KC. Comparison of landmark identification in traditional versus computer-aided digital cephalometry. Angle Orthodontist. 2000;70: 387-392.

15. Kamoen, L. Dermaut and R. Verbeeck, The clinical significance of error measurement in the interpretation of treatment results. European Journal of Orthodontics. 2001;23(5): 569-578.

16. Keim, R. G., et al. Orthodontic Practice Study, Part 1 Trends. Journal of Clinical Orthodontics. 2015;49(10): 625-639.

17. Wang CW, Huang CT, Hsieh MC, Li CH, Chang SW, Li WC, Vandaele R, Marée R, Jodogne S, Geurts P, Chen C, Zheng G, Chu C, Mirzaalian H, Hamarneh G, Vrtovec T, Ibragimov B. Evaluation and Comparison of Anatomical Landmark Detection Methods for Cephalometric X-Ray Images: A Grand Challenge. Transactions in Medical Imaging. 2015;34(9):1890-900.

18. El-Fegh, I., Galhood, M., Sid-Ahmed, M., Ahmadi, M. Automated 2-D cephalometric analysis of X-ray by image registration approach based on least square approximator. In: 30th International Conference of Engineering in Medicine and Biology Society - EMBS 2008. 3949–3952.

19. Rischen RJ, Breuning KH, Bronkhorst EM, Kuijpers-Jagtman AM. Records needed for orthodontic diagnosis and treatment planning: a systematic review. PLoS One. 2013;8(11).

20. Durão AR, Pittayapat P, Rockenbach MI, Olszewski R, Ng S, Ferreira AP, Jacobs R. Validity of 2D lateral cephalometry in orthodontics: A systematic review. Progress in Orthodontics. 2013; 14: 31.

21. Manosudprasit A, Haghi A, Allareddy V, and Masoud, M. Diagnosis and treatment planning of orthodontic patients with 3- dimensional dentofacial records. American Journal of Orthodontics and Dentofacial Orthopedics. 2017;151:1083-1091.

Appendices

Appendix A: Raw Coordinate Data

RAW X COORDINATES - iORTHO

ID	S_x	Na_x	Or_x	A_x	U1A_x	U1E_x	L1E_x	L1A_x	B_x	P_x	M_x	PO_x
A_00107	109.9	31.9	52.4	41	43.8	36.1	40.4	54.4	49.8	50.1	57.8	140
A_00211	115.5	36.1	56.5	40.3	46.2	37.2	41.1	52.3	47.8	43.4	51.7	145.7
A_00206	107.8	39.4	50.2	32.3	38.4	28.6	33.1	43.9	37.6	136	43.4	136.2
A_00309	105.8	22.9	83.8	33.8	37.1	27.6	32.1	47.5	44.4	46.1	53.6	136.8
A_00407	106.7	33	51.2	37.5	42.8	34.4	37.8	52.9	47.6	48.2	56	137.8
A_00411	111.5	58.8	54	41.9	47.6	39.1	42.5	56.6	52.1	51.8	60	145
A_00507	117.1	40.3	59.1	45.6	50.4	41.7	47.6	56.6	53.8	51.8	59.1	141.4
A_00607	109.6	37.8	56.6	43.1	47.4	41.5	46	56.9	53	53.8	61.4	136.7
A_1105	113.3	45.4	60.9	40.6	46.8	35	39.2	45.4	41.2	36.6	44	137.6
A_01207	109.9	31.9	52.4	41	43.8	36.1	40.4	54.4	49.8	50.1	57.8	140
A_01308	113.5	34.3	53.2	41.9	45.9	39.1	43.3	58.3	64.3	53.5	60.9	53.5
A_01304	106.7	32	47.6	37.4	40.5	33.1	37.1	51	45.3	45.6	52.7	132.5
A_1408	95.4	27.5	48	32.5	36.5	33.1	37.3	44.9	41.2	39.6	47.4	127.4
A_1607	93.1	18.5	37	22.4	29.2	18.5	23.8	38.1	34.8	119	46	118.9
A_01807	88	15.4	32.8	20.7	26.3	17.4	21.3	35.3	32.2	34.7	42.9	114.6
A_01811	90.9	17.1	33.4	21.9	28.6	18.2	23	38.1	35.1	39	46.6	117.8
A_01905	86.5	17.5	30.9	16.7	22	12.5	19.7	34.2	30.3	31.4	39.5	112.3
A_01912	87.2	16.5	30.8	13.7	17.9	8.4	12.3	28.8	25.2	25.7	33.3	111
A_02106	92.8	21.3	42.1	25.2	31.7	22.4	25.8	35.3	29.2	25	32.3	118.9
A_02410	93.3	20.4	35.7	22.3	26.5	19	22.9	39.6	34.9	37.1	45.2	116.2
A_02513	86.8	17	33.5	20.9	26.5	19	22	32.4	27.9	25.9	34	115.8
A_02609	91.7	18.4	33.2	21	25.1	18.2	22.8	37.5	32	33.2	42.1	120.5
A_02711	86.6	17.8	32.2	26	30.2	19.9	24.5	38.5	34.5	34.8	42.3	114.2
A_02811	86.4	10.1	29	20.3	25.2	17.4	21.5	37.7	33.6	33.1	40	113.1
A_03103	89.1	19.4	48	26.8	32.6	24.6	27.1	37.4	33.1	33.1	40.8	116.2
A_03206	87.9	13.7	34.3	20.3	25.1	23.1	27	36.8	32.8	33.4	40.8	115.6
A_03305	90	19.7	49.3	14.2	19.4	9.7	17.1	28.8	23.9	21.9	28.2	108.9
A_03401	84.5	15	28.1	21.6	27.2	18.4	24.4	34	33.2	31.5	38.8	109.2
A_03604	84.6	14.6	31.5	18.9	24.3	16.6	22.6	36.9	31.5	30	37.5	111.2
A_03007	93.8	14.8	32.3	20.9	25.7	17	20	35.3	30.1	33.6	41.4	123.9

RAW Y COORDINATES – iORTHO

	S_y	Na_y	Or_y	A_y	U1A_y	U1E_y	L1E_y	L1A_y	B_y	P_y	M_y	PO_y
A_00107	21.3	17.6	52.4	76	80	102.7	101	121	121	136.3	142.3	39
A_00211	17.3	12.3	41.7	74.9	75.2	98.4	41.1	113	112.4	129.9	136.2	36.4
A_00206	16.6	4.5	35.9	65.5	65.5	88.8	84.3	104.8	103.1	118.9	125.4	37.6
A_00309	18.4	8.7	58.9	79	81.8	106.9	103.8	124.5	126.2	144	150.2	35.7
A_00407	29.4	24.6	56.3	85.7	87.1	110.9	107.8	126.1	125.8	140.1	145.9	51
A_00411	16.3	22.5	49	80.8	82.5	106.7	104.2	122.5	121.9	139.7	145.9	38.3
A_00507	42.9	33.1	64.2	90.2	91.9	115.4	111.8	130	126.3	144.6	150.4	58.8
A_00607	41.2	33.9	64.4	92.2	91.6	115.7	111.5	129.1	128.6	142.6	147.6	54.9
A_1105	36.1	29.6	54.4	86.3	87.4	110.3	106.3	125.8	123.8	139.6	146.4	57.5
A_01207	21.3	17.6	52.4	76	80	102.7	101	121	121	136.3	142.3	39
A_01308	26.6	9.1	50.1	83.2	85.5	109.6	105.3	125.1	127.7	139.3	145	44.7
A_01304	24.9	18.1	46.4	74.7	78.7	102.8	98	118.1	117.5	129.9	135.6	40.5
A_1408	42.7	31.7	64.5	93.7	94.3	117	113.1	134.7	134.1	150.7	156.6	56.1
A_1607	51.6	40.4	74.1	101	101.9	128.5	123.5	140.9	142	155.4	160.5	67.6
A_01807	42	35	67.2	98.6	100.3	122.1	119	135.9	137.8	150.1	156.6	59.7
A_01811	37.6	28.9	60.9	92.9	94.3	118.1	116.4	133.3	135.5	149	154.9	55.6
A_01905	52.9	39.2	69.3	98.2	99.6	123.2	119.1	138.5	139.6	152.2	158	65.7
A_01912	51.2	33.3	64	93.7	96.5	118.6	117.7	135.9	137	152.4	158.8	65.4
A_02106	51.9	33.1	59.2	97.4	99.1	122.4	120.1	135.5	135	152.4	159.1	118.9
A_02410	33.8	22.3	56.4	86.8	90.7	117.2	115.3	133.1	136.8	153.2	158.8	51.9
A_02513	43.8	34.3	67.3	98.3	101	124.8	121.7	141.8	142.1	158	164.1	59.7
A_02609	36.9	23.2	60.2	91	94.3	120.5	115	137.2	138.2	151.6	158	52.2
A_02711	44.9	35.7	69	99.8	102.4	126.6	121.4	140.4	141.3	154.4	160.5	58.4
A_02811	40.6	30.7	66.1	95.6	96.5	123.2	119.4	140	140.3	154.2	160	58.8
A_03103	53.4	46.3	76.5	101.9	102.2	126.5	123.4	141.3	141.9	156.2	161.6	69.4
A_03206	49.4	45.4	74.3	100.3	100	126.5	122.3	141.7	141.4	154.4	159.4	64.8
A_03305	60.2	41.3	75.8	94.1	95.8	117.5	115.5	136	134.6	146.6	151.7	79.6
A_03401	62.7	57.6	81.1	107.8	106	124.2	121.9	138.7	138.7	146.6	151.7	78.8
A_03604	48.6	38.1	69.5	91.8	93.3	117	116.2	134.8	134.2	148.2	154.2	65.8
A_03007	35.4	32.3	60.3	93.9	94.8	120.5	115.7	134.9	134.1	153.3	158.5	49.8

RAW X COORDINATES – Webceph

ID	S_x	Na_x	Or_x	A_x	U1A_x	U1E_x	L1E_x	L1A_x	B_x	P_x	M_x	PO_x
W_00107	115.4	41.9	60.9	42.2	47.2	36.3	43.9	56.4	52.2	38.8	60.1	144.1
W_00211	122.6	52.7	65.1	45	52.4	41.9	47.6	58.3	51.8	49.8	56.9	154.6
W_00206	108.7	43	53.3	34.3	38.9	27.7	34	44	39.1	37.2	43.2	137.3
W_00309	105.1	32.8	50.7	31.7	37.1	27.9	33.9	46.6	44.2	46.1	54.2	135.5
W_0411	118	43	63.5	42.1	48	38.8	41.9	55.3	52	52.5	60.7	142.7
W_00407	109.3	39.9	59.2	37.5	43.7	34.5	38.8	52.5	46.6	49	57.3	138.7
W_00507	116.3	47.2	64.3	45	49.8	40.7	47.4	57.6	53.9	52.8	60.3	137.7
W_00607	110.3	45.5	59.2	44.1	47.4	40.6	46.3	57.3	54	53.5	61.2	134.7
W_01105	114.6	47.3	57.3	41.6	47.6	35.4	41.6	48.6	41.3	36.7	44.6	136.7
W_01207	108.9	30.9	49.4	39.2	40.9	35.1	38.6	52.8	47.6	47.8	56.9	140
W_01304	107.8	35.7	48.9	36.2	41.9	32.7	36.2	49.7	45.1	45.9	55.1	133.7
W_01308	114.5	41.8	55.3	40.1	47.1	38.4	42.4	53.9	61.7	64	76.3	142.3
W_01408	97.2	32.5	49	33.3	37.4	32.8	36.6	43.8	41.3	39.6	46.5	148.4
W_1607	93.2	24.3	41	23.5	27.3	17.8	24.3	37.4	35.5	38.5	45.9	38.5
W_01807	88.7	15.4	33.8	21.9	27.6	17.3	21.6	34.6	32.5	35.2	43.3	115.8
W_01811	91.4	18.1	35.9	22.6	26.5	18.4	23.4	36.5	36.8	38.2	47.1	117.8
W_01905	86.9	19.4	31.3	17.2	22.8	11.9	20.4	33.1	30	31.8	40.3	113.2
W_01912	88.5	19.3	28.6	12.6	18.5	7.6	12.9	27.7	24.9	25.2	33.1	113.7
W_2106	93.7	24.2	46.6	25.5	30.6	21.3	25.5	33.5	27.4	25	32.2	118.1
W_02410	94.4	25.8	35	22.7	25.5	18.8	22.7	35.6	35	36.7	44.8	116.8
W_2513	88.1	19.9	37.8	22.1	26.3	19.3	22.4	31.3	28.3	26.6	33.6	115.5
W_02609	91.6	19	35.2	20.2	25.8	17.2	23	36.4	31.4	32.1	41.8	119
W_02711	87	18.4	33.4	24.8	30.7	19.8	24.8	38.2	34.3	34.3	41.2	114.3
W_02811	87.2	16.7	36.9	19.6	22.8	18.2	20.9	35.6	32.1	33.4	39.9	113.8
W_03103	90	25.3	40.6	24.8	32.8	24.2	27.5	39.5	32	32.8	40.6	113.7
W_03206	88.9	20.4	47	24.4	25.8	22.9	26.6	36	30.3	32.8	41.1	112
W_03305	90.2	23.2	31.6	13.7	19	8.4	17.4	28.3	23.2	22.4	28.3	22.4
W_03401	85.8	18	42	22.1	29.9	18.8	24.9	35.4	30.2	30.7	37.9	108.4
W_03604	85.6	20.3	35.2	19.1	25.3	16.6	23.4	36.6	31.2	30.7	37.7	111.2
W_03007	94.2	20.3	35.4	21.1	26.3	16.8	21.7	34.3	32	33.7	41.4	123.1

RAW Y COORDINATES – Webceph

ID	S_y	Na_y	Or_y	A_y	U1A_y	U1E_y	L1E_y	L1A_y	B_y	P_y	M_y	PO_y
W_00107	21.2	21.8	50.3	80.2	82.4	106.2	105.1	124.3	126.3	138.6	147.5	45.5
W_00211	13	7.9	34.5	72.5	72.5	95.7	92.6	110.4	109.8	125.1	135.9	37.7
W_00206	16	8.2	33.4	65.8	66.9	88.3	84.8	102.2	103	114.7	123.9	40.8
W_00309	16.8	10	38.8	78.9	83.8	106	103.5	120.9	126	141.2	149.4	39
W_0411	16.3	13.5	39.6	81.2	82.4	105.1	103.7	120.3	123.4	139.7	145	38.2
W_00407	28.4	23.6	49.6	86	87.1	109.8	107.7	123.8	124.3	139.3	145.2	50.9
W_00507	44.5	34.8	58.9	90.8	92.7	114.7	112.8	130.2	131.5	144	150.8	59.5
W_00607	41.3	38.5	61.9	91.2	92.9	114.3	111.2	127.7	129.1	141.1	147.7	55.6
W_01105	35.9	22.1	56.2	85.1	86.4	109.4	106.7	127	124	136.7	144.8	60.8
W_01207	20.9	20	51.5	77	80	102.3	101.2	123	121.4	138.4	142.3	36.6
W_01304	24	17.6	43.8	78.9	78.3	102.1	98.6	117.2	117.2	129.9	138.1	43.8
W_01308	26.1	19.6	46	84.2	85.6	111.1	108.6	124.3	134.4	151	157.2	47.1
W_01408	43.2	33.9	64.4	92.8	94.1	117	113.4	132.4	135.4	148.4	156.1	60.8
W_1607	51.7	48.9	72.4	101.1	104.4	126.8	124.1	140	141.6	154.7	160.2	68.9
W_01807	41.7	36.3	65.5	98.2	98.5	120.7	118.2	133.9	137.5	149.1	155.9	60.6
W_01811	37.9	31.2	59.1	92.8	97.5	117	116.8	129.8	135.1	147.4	154.6	55.5
W_01905	52.8	42.4	69.5	97.3	99.7	121.5	119.3	135.8	137.6	150.9	157.5	68.4
W_01912	51.5	34.2	65.3	94.7	96.9	118.5	117.6	134.2	138.7	151.8	159.1	66.4
W_2106	51.6	39.4	68.4	98.2	99	121.6	120.5	138.6	136	149	158.9	70.8
W_02410	33.6	25.2	55.7	88	95.5	116.8	116.2	132.2	135.9	151.5	158.3	54.3
W_2513	43.3	34.4	62.1	98.7	101.8	1233.9	121.4	139	142.1	155.8	164.4	115.5
W_02609	36.9	19.2	59	93.3	94.6	119.9	116.4	135.1	136.6	149.8	157.6	54.1
W_02711	44.6	37.1	67.7	102	102.8	126.2	121.8	138.8	140.7	152.4	160.8	64.2
W_02811	39.4	38.6	64.4	95.3	97.2	124.1	120.6	136.6	138.8	152.1	159.1	59.5
W_03103	52.8	46.7	75.1	104.3	101.8	126	124	142.2	141	154.6	161.6	70.9
W_03206	49.5	47.6	73.6	100.2	103.3	126.3	122	139.3	138.4	151.5	159.4	64.8
W_03305	59.4	42.9	72.6	96.9	97.5	116.5	115.1	132.5	133.3	144.8	151.8	82.4
W_03401	63.6	52.6	80	106	104	124	122	136.4	138.3	146.6	152.7	81.9
W_03604	48.7	41.1	66.4	94.9	94.6	116.3	116.3	132.9	134	147	154.6	68.4
W_03007	34.3	32	60.6	94	95.7	119.7	115.7	133.1	136.8	150.5	158.5	53.1

RAW X COORDINATES – OrthoDx

ID	S_x	Na_x	Or_x	A_x	U1A_x	U1E_x	L1E_x	L1A_x	B_x	P_x	M_x	PO_x
O_00107	108.3	32.7	51.6	34.2	38.1	26.4	30.3	42.2	35.8	27.5	42.8	134.5
O_00211	124.7	55.2	63.3	48.2	54	42.9	47	60.7	53.7	49.6	56.6	153.8
O_00206	108.2	47.4	52.5	34	39.4	28.5	32.5	45.7	39.4	36.5	44.5	136.2
O_00309	106	36.2	57.3	33.1	37.1	28.2	31.9	49.3	45.3	46.7	54.4	136.3
O_00407	107.6	49.7	57.4	40.4	44.1	35	37.9	54.8	48.3	48.3	55.1	139.3
O_00411	110.4	38.9	58.9	44.3	48.6	40	42.9	57.5	51.2	51.2	59.2	144.5
O_00507	113.7	42.9	58.6	44.3	48.6	38.9	44.3	60.3	53.4	49.7	54.6	138.8
O_00607	108.4	42.7	62.2	42.7	47.8	41.3	45.3	60.8	53.2	53.5	59.7	135.8
O_1105	114.4	67	68.2	44.5	49.6	36.8	40.8	51.3	42.2	37.9	44.8	139.2
O_01207	108.3	32	50.2	40.1	41.2	36.5	38.9	53	47.6	47.9	57.4	140.2
O_01308	115.4	35.7	55.9	42.3	47.6	41.1	45.1	60.1	55.9	54.5	59.8	139.8
O_01304	107.8	39.2	51	36.6	42.1	34	36.6	52.2	46.1	45.5	51.3	131.1
O_1408	96	32.2	48.3	33.6	39.1	33.4	36.5	45.7	41.4	39.1	48.6	39.1
O_1607	93.4	24.4	39.3	24.4	42.1	24.4	18.9	29.8	36.7	39.3	47.6	117.8
O_01807	88.7	16.6	32.3	24.4	29.7	18	21.9	39.3	32.3	34.8	44.1	115.1
O_01811	93.1	19.9	36.1	26.5	31.9	18.5	23.6	40.1	36.1	37.6	48.4	118.7
O_01905	87.6	17.9	31.2	19	24.7	13	20.4	36.3	30.1	30.9	40.6	112.9
O_01912	88.7	18.3	35.8	16.9	22.3	8.9	14.3	29.2	25.2	25.2	31.5	113.1
O_02106	92.8	27.3	40.4	27.3	32.7	23.3	27.6	38.1	30.2	26.2	33.9	119.3
O_02410	87	15.5	37.2	21.1	25.1	19.4	22.2	34.4	27.6	26.5	34.4	115.5
O_02513	87	15.5	37.2	20.8	25.1	19.4	22.5	34.4	27	26.5	34.4	115.5
O_02609	91.7	19.5	35.6	20.2	26	17.7	23.2	36.9	31.8	32.3	41.9	119.3
O_02711	86.7	17.6	33.7	27	31.3	19.9	24.3	40.4	34.9	34.9	43.4	113.7
O_02811	86.6	15.4	32.5	19.5	24.8	18	21.9	39.3	32.5	32.5	40.5	113
O_03103	89.6	17.6	42.1	27.1	31.1	22.8	25.4	38.3	31.7	31.4	39.2	115.5
O_03206	81.3	13.2	24.7	8.2	13.7	7.5	24	22.4	16.2	14.5	21.7	107
O_03305	96	29.3	39.6	23.4	28.2	19.9	27.3	41	35.9	35.6	41.3	114.5
O_03401	81.4	13.3	31.6	17.2	22.8	12.5	17.8	32.4	23.6	24.4	31.8	104
O_03604	84.2	16.5	29.6	17	35.4	22	15.1	23.7	29.8	28.4	36.3	109.6
O_03007	95	17.2	36.1	22.3	27.5	17.2	20.6	38.1	32.6	34.6	41.2	122.5

RAW Y COORDINATES – OrthoDx

ID	S_y	Na_y	Or_y	A_y	U1A_y	U1E_y	L1E_y	L1A_y	B_y	P_y	M_y	PO_y
O_00107	32.2	23.9	56	81.9	82.5	105	105.3	82.5	124.2	141.6	147.5	56.3
O_00211	13.4	3.8	37.1	73	71.8	95.2	92.2	112.1	109.2	127	135.5	33
O_00206	16.3	4	34.8	65.4	63.9	87.9	83.9	103.9	101.3	115.9	123.9	37.7
O_00309	17.7	0.3	37.4	82.4	81	105.8	104.6	124.3	124.6	143.1	148.3	36.2
O_00407	30	23.5	54.8	85.3	85.3	109.1	107.7	125.2	125.2	139.6	145	51.2
O_00411	16	17.5	45.8	80.7	79.5	105.3	103.9	121.1	120.2	139.1	145.9	38.1
O_00507	42.6	33.1	63.7	90.8	89.4	113.4	11	130.5	128.8	139.4	150	58.3
O_00607	41.6	37.9	61.4	92.9	91.7	114.9	112.7	131.9	128.2	141.6	147.8	56.1
O_1105	35.9	39.9	53.3	85.8	86.1	108.3	105.5	130.3	121.5	134.9	145.1	57
O_01207	21	18	52.3	79.5	80.2	102.7	102.4	123.3	122.8	138.2	142.8	37
O_01308	26.4	14.2	49.1	84.8	83.1	109.2	104.9	122.2	125.1	137.6	144.4	44.2
O_01304	24.8	15.6	47.3	78.7	77.5	100.9	98.3	117.9	115	129.7	133.7	43.2
O_1408	42	34.2	63.9	91.2	91.2	114.2	112.4	132.9	132.9	148.2	154.5	54.4
O_1607	51.3	43.3	73.1	100	98.9	127.3	124.4	140.7	142.2	155.7	159.7	67.6
O_01807	41.5	36.5	66.8	97.9	98.2	121.5	119.3	136.1	136.4	147.9	154.9	60
O_01811	36.7	28.7	60.1	93.6	92.8	116.7	117	131.8	133.2	145.4	153.4	56.1
O_01905	52.2	41.7	68.1	99	98.4	121.4	118.8	139	137.6	150.9	157.4	65.2
O_01912	51.2	30.9	62.4	94.4	93.3	117.3	117.6	135.3	135.3	152.8	159.4	67.5
O_02106	51.5	42.4	71.2	98.8	97.3	121	121	142	140.3	151.1	157.7	64.6
O_02410	43.1	29.8	66.2	100	98.6	123.1	121.7	140.5	140.8	155.4	163.6	62.2
O_02513	43.1	29.8	66.5	100	98.8	123.1	121.7	140.5	140.5	155.4	163.6	155.4
O_02609	36.9	29.3	59.1	93.2	94.5	119.7	116.2	134.6	136.2	149.3	157.4	54.1
O_02711	45	34.3	66.8	102	100.5	125.1	122.5	138.8	139.7	153.5	159.1	59.8
O_02811	39.9	40.2	66.5	97.9	95.5	123	120.4	139	137.8	152.3	158.5	60
O_03103	54.4	47.8	72	103.1	100.5	125.3	124.1	144	141.1	155.5	161	72
O_03206	60.4	52.9	78.3	102.8	102	128	125.7	147.2	143.7	156.6	162.9	78.3
O_03305	52.1	43.6	70.4	94	92.3	115.4	111.9	131.9	129.6	142.7	147.8	70.1
O_03401	67.7	61.3	86	107.4	105.1	124.4	124.7	143.8	136.9	147.2	153.1	86
O_03604	49.9	39.3	67.8	94.8	135.8	116.3	116.3	92.1	133.1	147.8	154.5	67.8
O_03007	35.2	33.5	57.5	93.6	92.1	117.9	114.8	135.4	136.8	152.5	157.7	48.9

RAW X COORDINATES – CephX

ID	S_x	Na_x	Or_x	A_x	U1A_x	U1E_x	L1E_x	L1A_x	B_x	P_x	M_x	PO_x
C_00107	111	31.5	48.8	30.1	36.2	22.7	27.5	39.8	34.6	19.9	41.9	140.9
C_00211	116.6	35.3	52.6	33.9	40.1	31	35.9	46.1	39.6	36.7	46.6	148.4
C_00206	108.6	33.2	48.9	30.3	37.5	28.8	34	42.8	37.3	36.4	47.4	137.9
C_00309	104.7	22.6	40.5	31.8	36.6	26.8	31.5	45.5	44.9	45.5	56.4	136.8
C_00407	107.5	31.9	47.6	37.4	43.3	34.8	37.6	51	46.2	48.8	60.2	48.8
C_00411	109	29.5	46.4	30.1	36.9	25.5	28.9	40.5	35.3	34.1	43.9	139.4
C_00507	115	40	60.3	45	50.4	41	45.4	60.5	53.2	49.5	55.6	137.3
C_00607	114.3	37.9	57.4	41.8	48.6	36.3	40.9	47.8	41.8	38.5	51.4	140.2
C_1105	114.6	38.8	58.3	42.7	49.5	37.2	41.9	48.7	42.7	39.4	52.3	140.6
C_01207	108.5	33	51.7	41.2	42.5	37	39.2	54	50	48.6	57.9	140.3
C_01308	113.8	34.8	53.9	42	46	39.2	43.1	57.9	60.2	54.3	62	141
C_01304	110.1	34.8	51.2	36.8	43.6	34.5	36.4	49.9	46.3	45.5	51.5	131.3
C_1408	92.8	26.9	41.9	29.2	33.1	26.9	29.4	37.1	34	32	38.5	122.5
C_1607	88.9	17.4	32.6	15.7	21.3	9.9	16	29.8	26.8	28.7	26.5	114.6
C_01807	83.9	12.8	25.3	11.4	17.2	6.4	11.1	23.6	20.5	22.5	30.5	110
C_01811	87.9	16.2	28.4	16.2	21.6	9.9	14.7	30.1	25.2	28.1	36	113.7
C_1905	83.9	15.3	26.1	12.5	17.9	6.2	14.2	27.2	23.5	26.1	33.7	110.8
C_01912	88.2	17.1	30.5	15.4	20.4	10.1	14.8	28.3	28.3	28.3	39.5	116.3
C_02106	91.4	17.2	37	20.5	27.6	18.6	22.4	28.5	23.8	21.4	31.2	117.4
C_02410	92.3	18.2	33.3	17.6	22.9	15.1	19	31.3	28.3	31.9	43.4	114.5
C_02513	84.6	13.4	30.8	14	19.8	12.2	14.8	22.4	18.6	17.7	26.5	112.2
C_02609	89.5	16.2	29.5	14	20.2	10.9	16.7	28.3	23.6	23.9	33	117
C_02711	86	16.7	30.6	24.8	30.8	18.9	23.4	36.8	32.3	34.3	43.5	114.5
C_02811	82.1	8.6	22.7	9.7	15.4	5.9	8.6	22.4	18.9	17.7	25.1	107.8
C_03103	85.8	14.8	29.9	18.9	25.3	14.6	18.4	26.8	22.5	22.7	32.4	111.6
C_03206	82.4	9	24.7	9.8	14	6.7	12.6	19.9	15.7	15.7	23	108
C_03305	94.2	23.3	37.5	22.3	27.7	17.6	25.2	37.2	34.2	33.7	40.2	33.7
C_03401	84	15.1	30.8	18.8	28.5	18	24.3	35	30	30	36.8	109
C_03604	82	12.1	26	11.8	17.5	10.4	16.7	27.4	23.6	23	31.3	109.1
C_03007	89.4	10.4	27.8	11.4	16.4	4.4	9.5	23.4	18.3	19.9	27.5	118.4

RAW Y COORDINATES – CephX

ID	S_y	Na_y	Or_y	A_y	U1A_y	U1E_y	L1E_y	L1A_y	B_y	P_y	M_y	PO_y
C_00107	37.4	24.6	59.7	84.5	86.7	111.7	110.6	131.2	131.2	140.9	154.4	59.7
C_00211	25	17.1	45.1	81.4	80	104.4	97.8	119.4	116.8	135.3	142.3	45.4
C_00206	15.1	4.9	34.3	66.9	63.4	90.2	83.5	103.3	101.9	117.3	124	34.9
C_00309	17.6	11.2	43.5	79.3	79.6	108.9	103	123.1	134.5	144.3	148.2	35.5
C_00407	28.5	27.1	53.9	86.4	86.4	111.5	107.8	123.7	123.7	140.9	142.3	48.8
C_00411	29.5	22.1	52.8	86.6	85.4	112.1	107.5	127.1	125.6	145	150.8	52.8
C_00507	38.6	33.2	59.6	90.1	89.9	114	111.5	131.4	129	140	151.2	58.5
C_00607	34.6	24.2	54.7	86.6	86	110.2	105.3	126.1	122.3	137.7	143.7	55
C_1105	36.9	30	54.2	85.3	86.5	108.5	105.8	128	123.6	135.6	148.4	57.3
C_01207	21.3	18.5	52.9	77.5	81	103	102.8	121.4	122.3	138	144	36.9
C_01308	26.8	18.1	42.1	77.6	77.3	110	103	122.1	126.4	138	147.1	44.8
C_01304	25	13.6	39	78.8	77.6	99.2	98.8	115.8	115.6	128.9	134.5	43.6
C_1408	47.5	35.4	65.7	94.8	93.7	119.7	113.5	135.8	136.1	152.3	158.2	65.7
C_1607	57.7	44.7	74.6	102	102.5	130.4	124.3	142.8	145	159.1	162.4	74.6
C_01807	49.1	39.2	67.8	101	100.8	124.4	119.4	137.5	139.4	154.7	158.8	67.5
C_01811	43.4	31.8	61.8	94.7	94.7	120.5	117.7	135.8	137.5	153.4	157.4	61.5
C_1905	56.1	40.8	70	100	100.6	125	118.8	138.3	139.7	155.6	158.4	70
C_01912	49	31.1	61.9	93.8	95.8	119.9	116	133.6	141.7	151	157.4	62.2
C_02106	53.7	39.4	71.4	101	98.3	124.3	118.5	142.1	138.8	153	159	70.9
C_02410	36.4	24.3	55.4	89.6	89.6	118.4	115.6	134.9	134.6	154.5	158.7	55.4
C_02513	48.3	35.5	68	102	99.4	126.2	122.1	142.7	143.3	159.6	164.5	159.6
C_02609	42.2	30.3	59.7	94.9	95.7	122.3	116.5	137	138.7	155	160.3	60.2
C_02711	44	36.8	68.5	103	102.3	127.6	121.5	139.6	139.3	155.2	160	57.7
C_02811	48.1	39	67.9	97.8	97.8	125.2	121.1	139.7	141.5	156.8	162.1	67.6
C_03103	59.3	47	75.1	105	104	129.2	124.1	144.1	142.8	158.9	163	158.9
C_03206	59.2	48.2	76.8	103	101.5	129.6	122.5	144.4	143.9	158.4	162.9	76.8
C_03305	54	41.3	70.3	94.5	93.4	118.3	112.1	131.1	132.5	145.8	148.8	70.6
C_03401	63	58	81.3	108	104.8	124	123	138.5	137.3	146.8	151.2	79.9
C_03604	52.9	40.3	69.9	97.6	97.1	119.3	116.8	134.3	134.3	150.2	156.3	69.9
C_03007	43.9	34.7	61	95.1	97	122.2	115.9	138.7	139.9	157	161.1	61

Appendix B: Abbreviation Key

2D: Two-dimensional

3D: Three-dimensional

AI: Artificial Intelligence

CWRU: Case Western Reserve University

Appendix C: IRB Approval



IRB Administration Offices
UH IRB Phone: 216.844.1529
CWRU IRB Phone: 216.368.6925

NOT HUMAN RESEARCH

Principal Investigator:	Tarek ElShebiny
Title:	Assessing the Accuracy and Reliability of Cephalometric Tracing Using Artificial Intelligence Modalities in Six Software Programs
IRB Number:	STUDY20231626
IRB Office:	CWRU IRB
Determination Date:	4/30/2024
Type of Submission:	Initial Study
Type of Review:	Determination
Documents Reviewed:	• Not Human Research , Category: IRB Protocol;

The IRB determined that the proposed activity is not research involving human subjects. **IRB review and approval is not required.**

This determination applies only to the activities described in the IRB submission and does not apply should any changes be made. If changes are being considered and there are questions about whether IRB review is needed, please submit a new study to the IRB for a determination.